ORGANIC CHEMISTRY FRONTIERS

RESEARCH ARTICLE

View Article Online
View Journal | View Issue

Cite this: *Org. Chem. Front.*, 2025, **12**, 6841

Monodentate halogen bond activation of aziridines in formal [3 + 2] cycloadditions

Mattis Damrath and Boris J. Nachtsheim *

Received 5th August 2025,
Accepted 16th September 2025

DOI: 10.1039/d5qo01119a

rsc.li/frontiers-organic

The ring opening of aziridines to produce various N-heterocycles traditionally requires strong Lewis acids or transition metal catalysts, with non-covalent organocatalytic approaches remaining largely unexplored. Herein, we demonstrate that N-heterocyclic iodonium salts can effectively catalyze [3 + 2] cycloadditions of aziridines through a monodentate halogen bond (XB) activation. Using 1–5 mol% of the iodolium catalyst, a wide range of aziridines undergo an efficient cycloaddition with a variety of dipolarophiles (carbonyls, alkynes, and alkenes) to furnish oxazolidines, pyrrolines, and pyrrolidines. DFT calculations revealed a previously underexplored *N*-activation mode, with detailed non-covalent interaction analysis showing that the N-heterocyclic iodonium salt's exceptional performance stems from combined I–N and I–π interactions.

Introduction

Non-covalent interactions have been demonstrated to play a hitherto unparalleled role in the supramolecular assembly of proteins,[1–4] in enzymatic reactions,[5–7] as well as in drug design and material science.[8–15] Among the extensive array of non-covalent interactions, hydrogen bond donors have shown notable efficacy in their role as organocatalysts, facilitating a diverse spectrum of reactions.[16–21] In recent years, halogen bond (XB)[22,23] and chalcogen bond (ChB)[24] donors have emerged as significant contributors to the field of organocatalysis.[25–32] Also, these compounds have been recognized for their substantial contributions in crystal engineering,[33,34] molecular recognition,[35,36] and in medicinal applications.[37,38] The restriction of reactivity imposed by non-covalent interactions delineates the constraints of this catalysis discipline, particularly regarding the limitations of activation targets and reaction patterns. Despite the capacity of halogen or chalcogen bond donors to activate a variety of molecules, including carbonyl compounds,[39–42] imines,[43] and nitroolefins,[44–46] their application has recently been extended to more challenging substrates such as esters,[47] alkenes,[48] alkynes,[49] and even carbene precursors.[50,51] Nevertheless, the activation of strained heterocycles such as aziridines remains a formidable challenge, as these transformations have historically relied on strong Lewis acids, transition metals, or high temperatures (Scheme 1A).[52–55] In 2022, Wang and co-workers presented the first example of a bidentate selenium(II) catalyst for the non-covalent activation of aziridines in a [3 + 2] cycloaddition (Scheme 1B).[56] They demonstrated the ability to obtain different N-heterocycles by altering the dipolarophile from alkenes to alkynes and carbonyls in good yields. Further

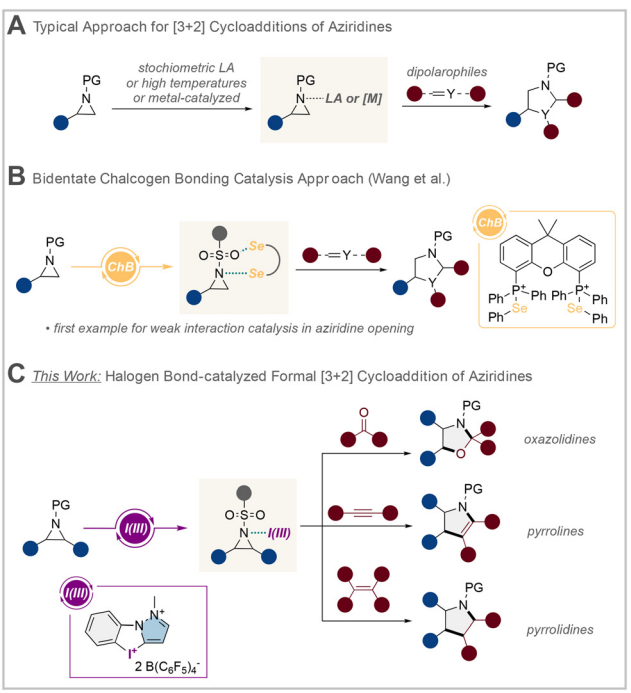

Scheme 1 (A) Typical approach for the activation of aziridines by strong Lewis acids, transition metals, or elevated temperatures. (B) First example of non-covalent organocatalysis for the ring opening of aziridines by a bidentate chalcogen bond catalyst by Wang and co-workers. (C) This work: XB-catalyzed [3 + 2] cycloaddition of aziridines with carbonyls, alkynes, and alkenes.

Institute for Organic and Analytical Chemistry, University of Bremen, 28359 Bremen, Germany. E-mail: nachtsheim@uni-bremen.de

NMR experiments demonstrated that a cooperative Se–O and Se–N activation, facilitating the bidentate mode, in conjunction with the precise distance between the two selenium units, was instrumental in achieving the desired outcome. In a recent study, Tan and co-workers introduced a novel class of bidentate organotellurium catalysts, which demonstrated remarkable efficacy in the activation of various azetidines and aziridines for the cycloaddition with alkenes and alkynes.[57]

Given the well-established fact that XB-donors facilitate significantly more robust activation than their chalcogen analogs, our research group was intrigued by the question of whether hypercoordinated iodine compounds,[58–64] especially our previously developed N-heterocyclic iodonium salt XB catalysts,[65–67] would also allow an effective activation of aziridines for [3 + 2]-cycloadditions.

In the present work, we demonstrate that such an activation by a monodentate XB catalyst is a straightforward process that allows the synthesis of a variety of oxazolidine, pyrroline, and pyrrolidine scaffolds from *N*-sulfonyl aziridines.

Results and discussion

Reaction development

Initially, the reactivity of this activation process by halogen bonding was evaluated through the investigation of the well-established monodentate XB catalysts **1a–e** in the ring opening of *N*-tosyl-protected aziridine **2a** with cyclohexanone (**3a**) to obtain oxazolidine **4a** (Scheme 2). Initial preoptimizations with catalyst **1a** (see SI) revealed that a catalyst loading of only 1 mol% of the XB-donor in DCM was sufficient to successfully synthesize the target compound **4a** in a nearly quantitative yield after 2 h.

After implementing the aforementioned conditions, a ^{1}H-NMR kinetic study was conducted with all well-established catalysts **1a–e**.[42,65–67] This kinetic study revealed that catalyst **1a** exhibited the highest level of activity, surpassing all the other iodonium salt catalysts. It should be noted that the N-heterocyclic iodonium salt catalysts **1b** and **1d** have shown comparable conversion rates to each other and provided good yields of about 80% after 4 h reaction time. It is also noteworthy that the *C*-bound pyrazole **1c** exhibited a significant decrease in activity, with a yield of only 22% after the specified time, while using the simple iodolium salt catalyst **1e** resulted in almost negligible product formation.

The observed effectiveness of these catalysts in activating aziridines aligns with the relative Lewis acidity strength of the tested monodentate iodonium salts, with higher acidity generally producing better results.[68] This observation suggests that the efficiency of the halogen bond-catalyzed reaction depends heavily on the strength of the catalyst's Lewis acid properties. To further verify the relevance of the XB for the catalytic activation, the reaction was carried out with catalyst **1a** in the presence of 10 mol% NBu_4Br. This experiment resulted in no product formation, indicating an XB-mediated activation of the aziridine **2a**.

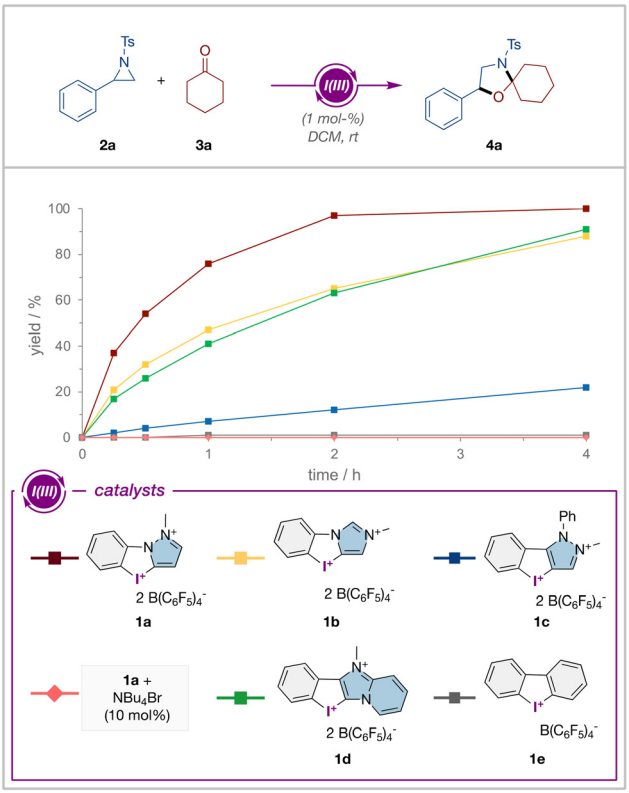

Scheme 2 ^{1}H-NMR kinetic studies for the cycloaddition of aziridine **2a** with cyclohexanone (**3a**) employing various iodine(III) XB-donors **1a–e**. General reaction conditions: **2a** (0.100 mmol, 1.0 eq.), **3a** (3.0 eq.), XB catalyst **1** (1 mol%), DCM (0.1 M), rt.

After establishing the aforementioned conditions, other substrates were investigated. Through time-dependent ^{1}H-NMR spectroscopy, we could prove that when utilizing benzaldehyde (**3b**) as a coupling partner, a complete conversion to oxazolidine **4b** could be obtained after a reaction time of approximately 30 min (Scheme 3A).

This reaction exhibited a diastereomeric ratio (dr) of 92 : 8, in favor of the *cis*-isomer (***cis*-4b**).[69] We also observed that as the reaction continued, the diastereomeric ratio underwent a shift. After a reaction time of 1 h, a commendable dr of 90 : 10 was obtained; however, after 2 h, a ratio of 78 : 22 was already observed, which resulted after 4 h in a final dr of 45 : 55, with the ***trans*-4b** isomer being slightly favored. The experiment provided clear evidence that the initial kinetic preference is gradually overridden as the catalyst continues to mediate reversible ring-opening/ring-closing sequences, ultimately approaching thermodynamic equilibrium where the slightly more stable ***trans*-4b** isomer marginally predominates. To further verify the observed behavior, we repeated the reaction but added NBu_4Br (10 mol%) after an initial reaction time of 15 min (Scheme 3B). Analysis of the ^{1}H-NMR spectra over a 3-hour period clearly showed that addition of the Lewis base completely halted the reaction. This confirms our hypothesis that catalyst **1a** causes the observed time-dependent conversion between diastereomers. It also highlights the importance

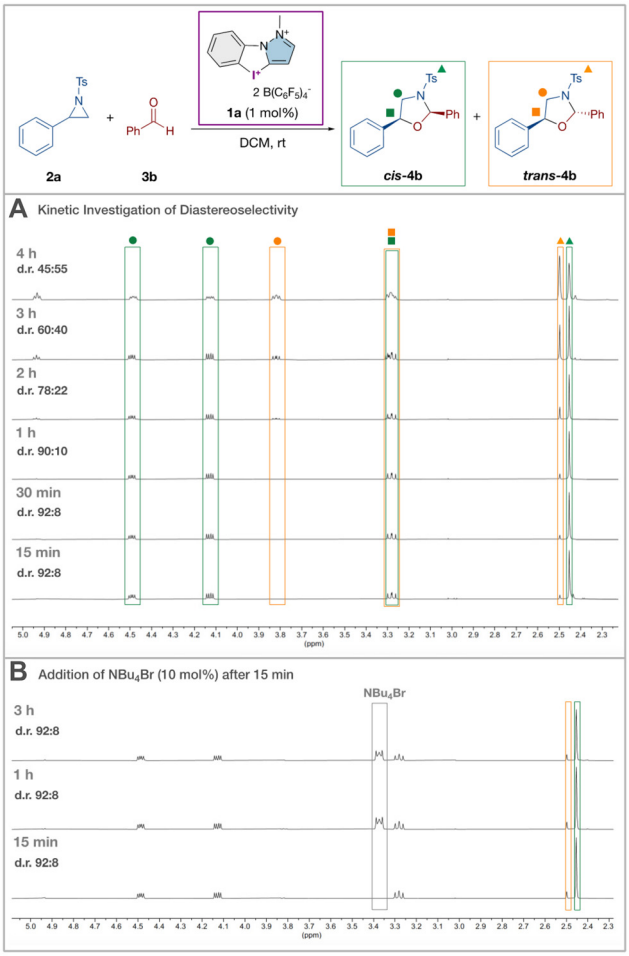

Scheme 3 XB-catalyzed cycloaddition between aziridine **2a** and benzaldehyde (**3b**) with **1a** as the XB donor. General reaction conditions: **2a** (0.100 mmol, 1.0 equiv.), **3b** (3.0 equiv.), **1a** (1 mol%), DCM (0.1 M), rt. (A) Kinetic investigation of diastereoselectivity. (B) Kinetic investigation with the addition of NBu_4Br (10 mol%) after 15 min.

of continuous reaction monitoring to properly determine the scope of suitable substrates.

Scope of the reaction with carbonyls

With this information in hand, the reaction of aziridine **2a** with benzaldehyde (**3b**) was terminated after 30 min with an excellent yield of 93% and 92 : 8 dr for the target oxazolidine **4b** (Scheme 4). With sterically hindered 2-methylbenzaldehyde (**3c**), we observed a significant decrease in the conversion rate. After 24 h, oxazolidine **4c** could still be obtained in 85% yield with an improved diastereoselectivity of >95 : 5. The cycloaddition of **2a** with the electron-donating 4-methoxybenzaldehyde (**3d**) yielded the desired oxazolidine **4d** after 30 min in nearly quantitative yield of 96% but with no diastereoselectivity. The electron-withdrawing nitro-substituted oxazolidine **4e** was also accessible under the investigated reaction conditions with 90% yield and 95 : 5 dr after 2 h. Next, we focused on aromatic carbonyl compounds. Acetophenone, indanone, and benzophenone proved to be suitable coupling partners for the cycloaddition of aziridine **2a**, with yields of up to 97% and up to 75 : 25 dr for the oxazolidines **4f–4h**. We also conducted the cycloaddition with acetone, which resulted in a comparable and nearly quantitative yield of 99% for **4i**. Using *N*-methylisatin (**3j**) as the substrate, the reaction time increased to 24 h with a moderate yield of 62% and 3.5 : 1 dr for the desired spirocycle **4j**.

Next, a variety of aziridines were investigated under our reaction conditions with cyclohexanone as the coupling reagent. First, various protecting groups on the aziridine moiety were compared, and it was found that both the Nosyl (Ns) and Mesyl (Ms) protecting groups could be used, although significantly longer reaction times were required compared to the Tosyl protecting group, and lower yields for **4k** and **4l** of 64% and 91% were observed. Other protecting groups, such as Acetyl or Boc, did not show any reactivity under the reaction conditions investigated. Concerning the substitution on the aromatic skeleton of the aziridine, electron-rich, electron-poor or slightly sterically demanding derivatives **4o–s** were accessible in yields of up to 96%.

Aliphatic aziridines, such as **2t** and **2u**, could also be converted *via* XB-catalysis in the cycloaddition, but yielded oxazolidines **4t** and **4u** in significantly lower yields of 44% and 73%. Herein, we observed the formation of several by-products, including the ring-opening of the oxazolidine, which are likely attributable to the extended reaction times of 6 h and 24 h. The indene-derived aziridine **2v** could again be converted to oxazolidine **4v** in a short reaction time with a high yield of 95%, which indicates the requirement of the aromatic functionality of the aziridine for a fast and effective reaction outcome. The more activated aziridines **4w** and **4x** were unsuitable substrates. In both cases, known Lewis acid-mediated rearrangements occurred (see SI). Even adjusting the reaction conditions, such as lower temperatures or an increased catalyst loading, did not allow a successful reaction. To gain deeper insights into this reaction's regioselectivity, we conducted the cycloaddition of aziridine **2y**. We were able to separate the two resulting regioisomers **4y** and **4z** in 31% and 19% yield, respectively, with the higher substituted one as the expected major regioisomer.

Notably, our reaction protocol also worked well for opening the four-membered ring compound azetidine **5**. When combined with benzaldehyde, this reaction produced oxazinane **6** with good stereoselectivity (single diastereomer) and yield (75%).

Scope of the reaction with alkynes

Beyond creating oxazolidines **4** from aziridines **2** and carbonyls **3**, we found that our established reaction conditions also effectively promoted the cycloaddition between aziridines and alkynes **7** to form pyrrolines **8** (Scheme 5). Indeed, the reaction with phenylacetylene with **2a** afforded the desired pyrroline **8a** in an excellent yield of 91%. To further extend the range of aryl alkynes, various substituents on the aryl skeleton were investigated under the reaction conditions. While slightly sterically-hindered or electron-donating alkynes could be efficiently

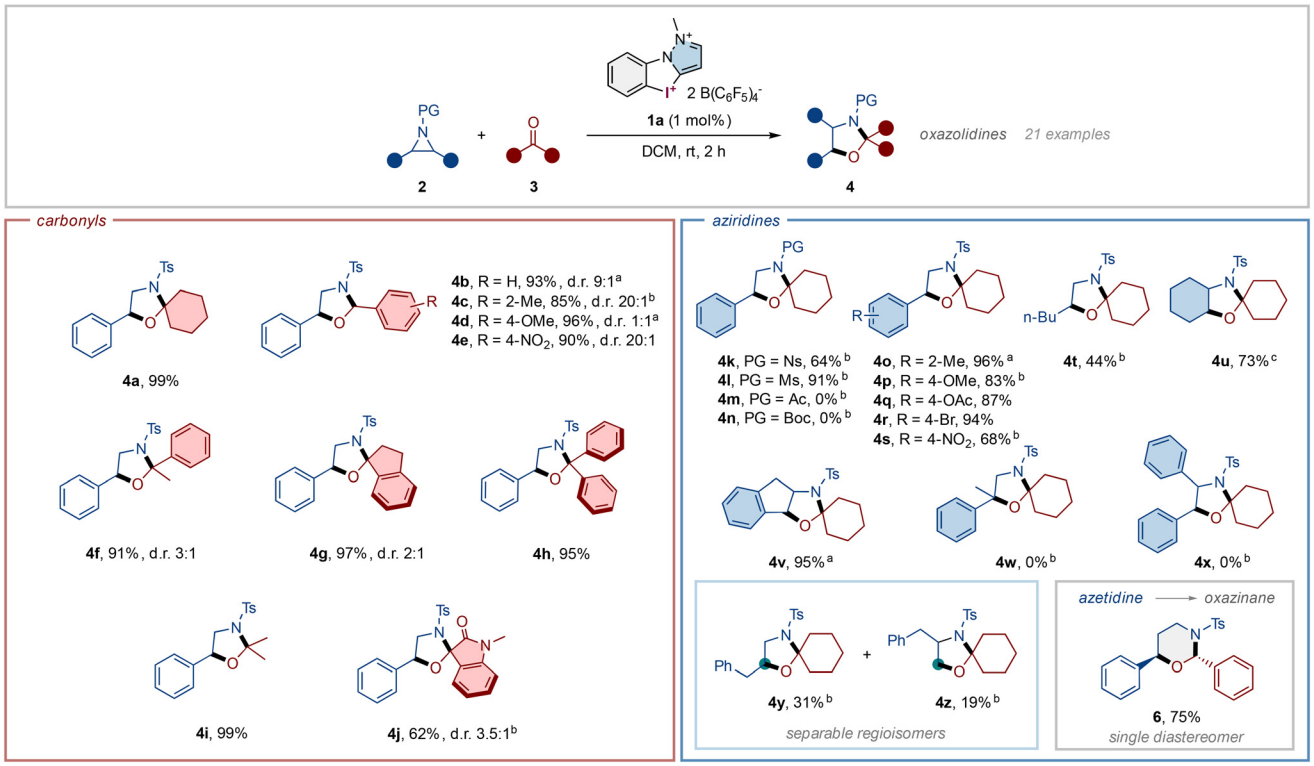

Scheme 4 Substrate scope for the XB-catalyzed cycloaddition of aziridines **2** and carbonyls **3** toward oxazolidines **4**. General reaction conditions: **2** (0.100 mmol, 1.0 equiv.), **3** (3.0 equiv.), **1a** (1 mol%), DCM (0.1 M), rt. [a] Reaction time: 30 min. [b] Reaction time: 24 h. [c] Reaction time: 6 h.

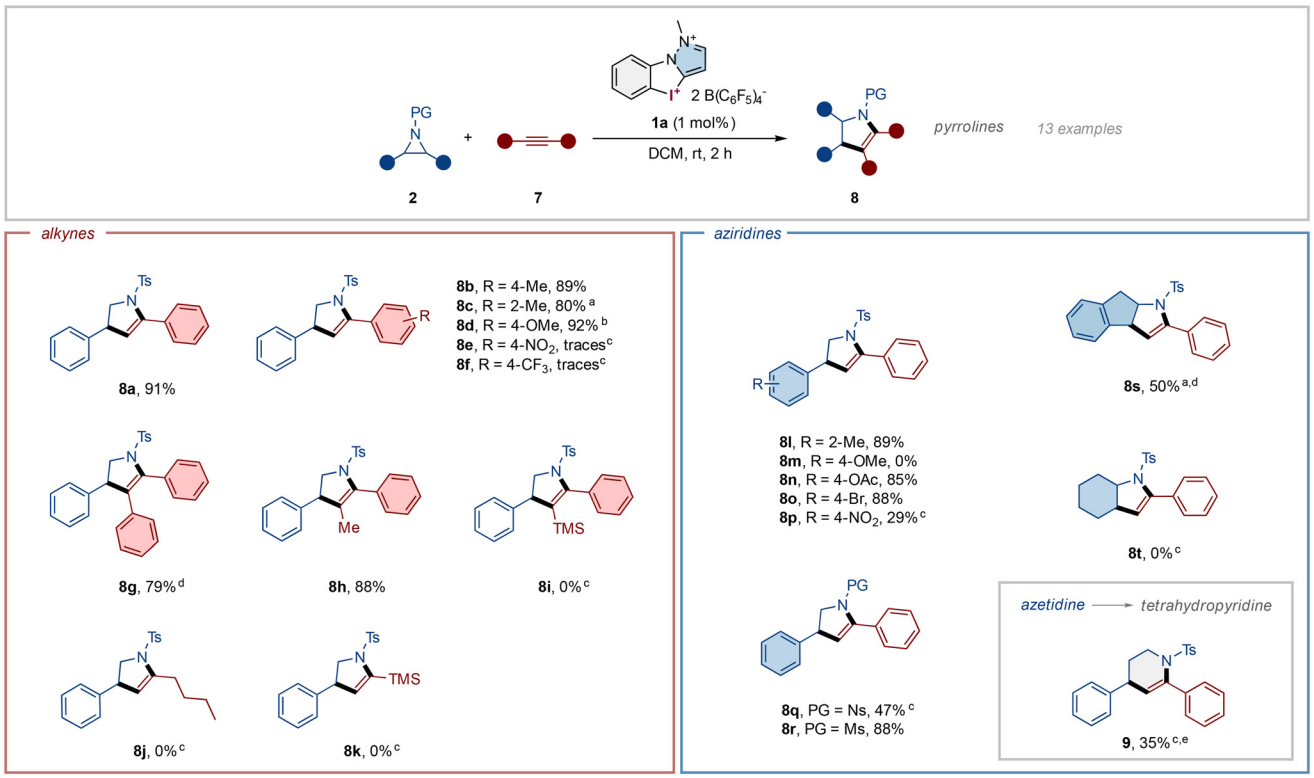

Scheme 5 Substrate scope for the XB-catalyzed cycloaddition of aziridines **2** and alkynes **7** toward pyrrolines **8**. General reaction conditions: **2** (0.100 mmol, 1.0 equiv.), **7** (3.0 equiv.), **1a** (1 mol%), DCM (0.1 M), rt. [a] **1a** (5 mol%) was used. [b] Reaction time: 30 min. [c] Reaction time: 24 h. [d] Reaction time: 1 h. [e] Reaction temperature: 50 °C.

converted to the desired pyrrolines **8b–d** in yields of up to 92%, the use of electron-deficient alkynes afforded only traces of the target compounds **8e** and **8f**. Furthermore, diphenylacetylene and 1-phenylpropyne were identified as suitable coupling reagents, yielding the corresponding pyrrolines **8g** and **8h** in 79% and 88% yield, respectively. The limitations of the method could be demonstrated through the utilization of alkyl or TMS-substituted derivatives, which are less activated or sterically hindered. Using these alkyne derivatives to potentially give pyrrolines **8i–k** resulted either in complete absence of product formation or yielded inseparable mixtures of compounds, demonstrating the limitations of this methodology with sterically hindered or electronically deactivated substrates. In the context of the aziridine scope, the evaluation of various aromatic substituents on the aziridine skeleton was conducted. The employment of the slightly sterically-hindered 2-methyl-substituted aziridine proved to be efficient within the reaction conditions, and the product **8l** could be obtained in a yield of 89%.

The formation of the highly activated pyrroline **8m** was unsuccessful due to product decomposition in the purification process. Pyrrolines **8n** and **8o**, containing OAc- or Br-substitutions, were obtained in yields of 85% and 88%. In contrast, the electron-deficient NO_2-substituted derivative could only be accomplished in a yield of 29%. After an extended reaction time of 24 h. The efficacy of alternative protective groups was also demonstrated, exhibiting a reaction behavior analogous to that observed with carbonyl derivatives. The Ns-protected pyrroline **8q** and the Ms-protected derivative **8r** could be isolated in yields of 47% and 88%. The pyrroline **8s** was accessible under the developed reaction conditions, but only in a moderate yield of 50%. Our method showed clear limitations when applied to aliphatic aziridines like the cyclohexene-derived compound, as we detected no formation of the target pyrroline **8t**. Similar to our earlier findings with carbonyl compounds, we found that azetidine **5** (the four-membered ring analog) could react with phenylacetylene to produce tetrahydropyridine **9**, though with only 35% yield.

Scope of the reaction with alkenes

Inspired by the study conducted by Wang and co-workers,[56] we also investigated the ring opening of aziridines with alkene compounds to obtain pyrrolidines. Initial experiments conducted under the previously utilized reaction conditions with aziridine **2a** and styrene (**10a**) yielded low yields of the desired compound, accompanied by long reaction times and the formation of multiple side products. Increasing the catalyst loading to 5 mol% effectively addressed the aforementioned issues, thereby enabling the exploration of a substrate scope for the cycloaddition of aziridines with alkene derivatives. Unlike the cycloadditions with carbonyl compounds, we found that diastereoselectivity could not be controlled in these reac-

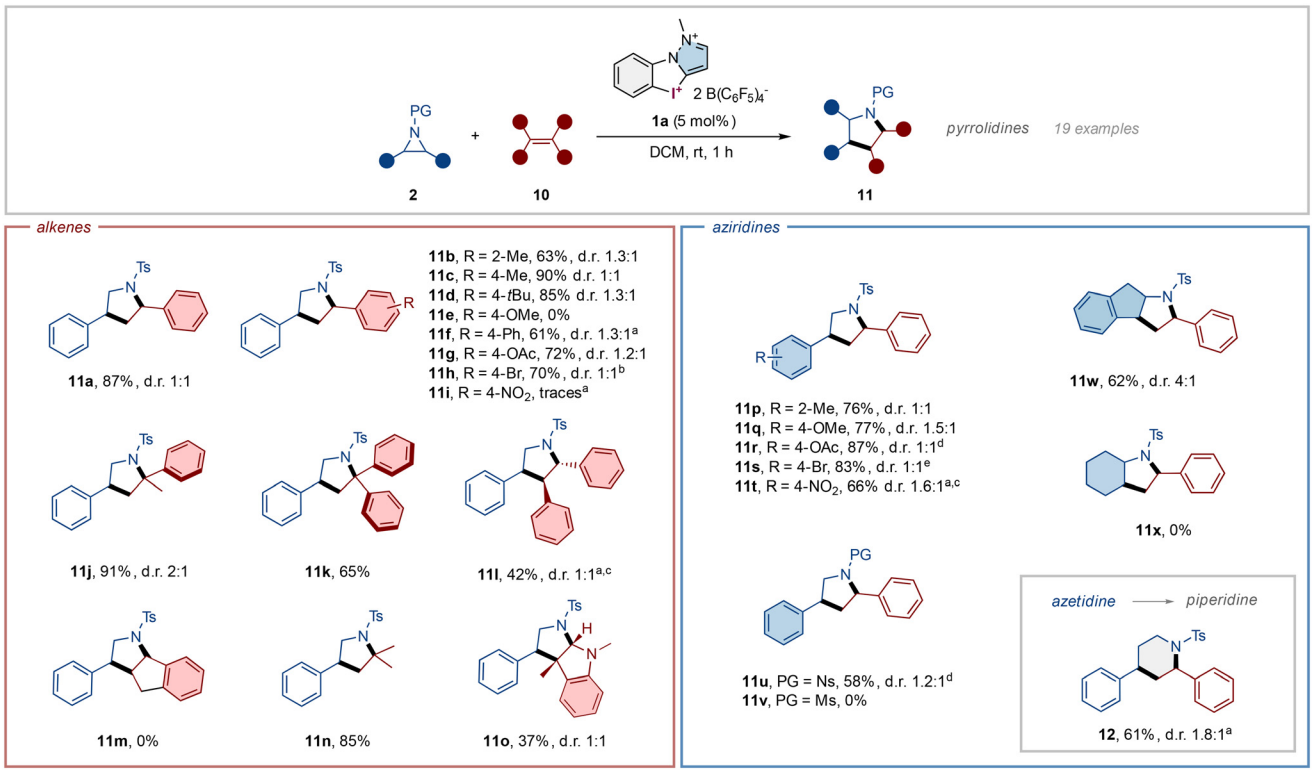

Scheme 6 Substrate scope for the XB-catalyzed cycloaddition of aziridines **2** and alkenes **10** toward pyrrolidines **11**. General reaction conditions: **2** (0.100 mmol, 1.0 equiv.), **10** (3.0 equiv.), **1a** (5 mol%), DCM (0.1 M), rt. [a] Reaction time: 24 h. [b] Reaction time: 2 h. [c] Reaction temperature: 50 °C. [d] Reaction time: 4 h. [e] Reaction time: 8 h.

tions. ^{1}H-NMR monitoring revealed that both diastereomers formed in nearly equal amounts right at the beginning of the reaction. For example, the initial reaction of aziridine **2a** with styrene (**10a**) afforded a promising yield of 87% and 1 : 1 dr for the desired pyrrolidine **11a** after 1 h reaction time (Scheme 6).

In the following, we started our investigation by examining various aromatic substituents on the styrene derivative to induce a potential diastereoselectivity characterized by electronic or steric properties. Using the sterically-hindered 2-methylstyrene, pyrrolidine **11b** was obtained in 63% yield with 1.3 : 1 dr, indicating a negligible impact of steric substituents on diastereoselectivity. Furthermore, *para*-alkyl substituted pyrrolidines **11c,d** were generated in high yields of up to 90%, while the strong electron-donating methoxy substituted derivative **11e** was unsuitable due to its rapid polymerization. Other *para* substituents such as Ph, OAc or Br afforded the desired products **11f–h** in up to 72% and up to 1.2 : 1 dr. The strong electron-deficient pyrrolidine **11i** could only be detected in traces after an extended reaction time of 24 h. Subsequently, the focus shifted to the investigation of substitutions on the exocyclic double bond of styrene. For trisubstituted pyrrolidines **11j–l**, yields ranged from 42% to 91%. In case of indene

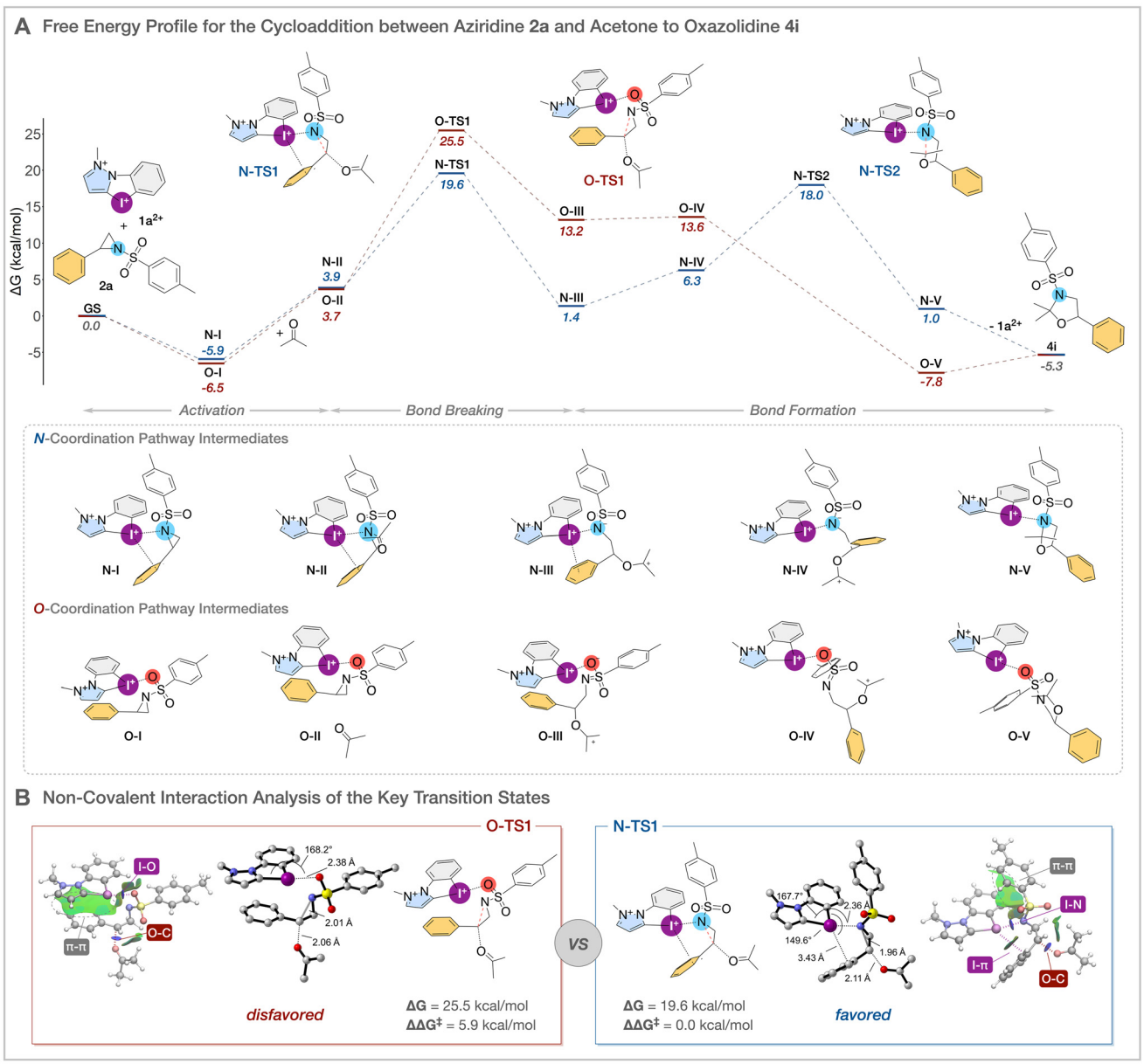

Fig. 1 DFT computations of the key intermediates for *O*- and *N*-activation at the ωB97X-D3BJ/def-2 TZVP (SMD18, DCM)//ωB97X-D3BJ/def-2 SVP (SMD18, DCM) level of theory at 298 K. (A) Free energy profile (in kcal mol^{-1}) for the cycloaddition between aziridine **2a** and acetone to oxazolidine **4i**. (B) Non-covalent interaction analysis of the key transition states. Color code for NCI plots: red = repulsion, green = van der Waals attraction/weak interaction (*e.g.*, hydrogen bonding, halogen bonding), blue = strong interaction (*e.g.*, hydrogen bonding, halogen bonding).

as the dipolarophile, an inseparable mixture of the product **11m** and the non-cyclized derivative was obtained (see SI). As an example of alkyl substitution, the reaction with isobutene yielded dimethylpyrrolidine **11n** in 85% yield. It was also possible to convert 1,3-dimethylindole as an alkene source under the developed conditions, leading to hexahydropyrrolo[2,3-*b*] indole **11o** in 37% yield and with 1 : 1 dr, whose core structure plays a relevant role in biology and pharmacology.[70]

Next, we focused on the conversion of various aziridines. Both electron-donating and electron-withdrawing aromatic substituents have shown good performance with yields ranging from 68% to 87% and up to 1.6 : 1 dr for pyrrolidines **11p–11t**, indicating a minor influence on the diastereoselectivity by these substituents. Regarding the protecting groups, the Nosyl-protected pyrrolidine **11u** was accessible in a moderate yield of 58%, while the Mesyl-protected derivative **11v** was unstable during the purification process. Trisubstituted pyrrolidine **11w** was synthesized in 62% yield with 4 : 1 dr, whereas the cyclohexene-derived aziridine showed no conversion toward **11x**. As with the other coupling reagents, styrene could also be converted with azetidine **5** in a formal cycloaddition to piperidine **12** in a yield of 61% and 1.8 : 1 dr.

Computational investigation

To gain insight into the coordination of the N-heterocyclic iodolium catalyst **1a** (N- *vs.* O-coordination) to the substrate and the origin of the high activity of this catalyst, DFT calculations were performed on the halogen-bond catalyzed formal cycloaddition between aziridine **2a** and acetone (Fig. 1). Free energies obtained at the ωB97X-D3BJ/def-2 TZVP (SMD18, DCM)//ωB97X-D3BJ/def-2 SVP (SMD18, DCM) level of theory at 298 K were used for the discussion (see SI for further details). The coordination of the catalyst $\mathbf{1a}^{2+}$ to the aziridine **2a** results in the formation of two complexes, **N-I** and **O-I**, that were found to be energetically very close, with a slight preference for the O-coordination of 0.6 kcal mol^{-1} (Fig. 1A).

Following the incorporation of acetone into the activation complex, the disparity between the two intermediates, **N-II** and **O-II**, diminishes to 0.2 kcal mol^{-1}. The XB-catalyzed bond-breaking process then occurs *via* **N-TS1** (19.6 kcal mol^{-1}) or **O-TS1** (25.5 kcal mol^{-1}) to yield the dipole intermediates **N-III** (1.4 kcal mol^{-1}) and **O-III** (13.2 kcal mol^{-1}). This substantial discrepancy in the transition state energies prompted further investigation into the behavior, which was subsequently analyzed in detail using the non-covalent interaction analysis (NCIPlot) method (Fig. 1B). This analysis clearly demonstrates that **O-TS1** interacts through an I–O interaction (2.38 Å), as well as a pronounced π–π interaction between the aromatic part of the iodonium salt and the aromatic unit of the aziridine. In contrast, **N-TS1** exhibits, in addition to these interactions, a further I–π interaction (3.43 Å) with the second σ-hole of the catalyst toward the aromatic skeleton of the aziridine. This interaction, in combination with the presumably better stability between the negative charge on the nitrogen and the positive one on the catalyst (ion pair), clearly favors the latter transition state ($\Delta\Delta G^{\ddagger}$ = 5.9 kcal mol^{-1}). This hypothesis is further substantiated by the resulting dipole intermediates, where the observed difference increased to 11.8 kcal mol^{-1}. A comparison with iodolium salt **1e**, which is experimentally inactive, reveals endergonic activation energies and significantly higher transition states (see SI for further discussion), yet the interaction behavior is the same for both pathways.

Subsequent rotations to **N-IV** and **O-IV** enable the following ring closure step. In the case of O-coordination, this intermediate can be converted barrierless into the stable catalyst-product complex **O-V** (−7.8 kcal mol^{-1}). In the case of the N-coordinated reaction pathway, the barrier for bond formation is predominantly attributable to the increased stability of the dipole intermediate due to the previously mentioned ion pair. This bond formation transition state **N-TS2** with a free energy of 18.0 kcal mol^{-1}, subsequently results in a stable catalyst-product complex **N-V** (1.0 kcal mol^{-1}). Decomplexation yields the oxazolidine **4i** (−5.3 kcal mol^{-1}) and regenerates the catalyst $\mathbf{1a}^{2+}$. In summary, the favored N-coordination pathway demonstrates a rate-determining step (RDS) barrier of 19.6 kcal mol^{-1} and is exergonic by 5.3 kcal mol^{-1}.

Conclusions

In conclusion, a straightforward method for the synthesis of various five-membered N-heterocycles from aziridines *via* XB-catalyzed [3 + 2] cycloadditions through monodentate activation is presented. *N*-Sulfonyl-protected aziridines have been shown to efficiently react in a formal [3 + 2] cycloaddition with carbonyls, alkynes, or alkenes as dipolarophiles in high yields and partially controllable diastereoselectivity. The exceptional performance of the N-heterocyclic iodonium salt catalyst as the XB-donor was ascertained through DFT calculations of the reaction pathway and an examination of the non-covalent interactions in the bond-breaking process. The monodentate N-coordination pathway, which has emerged as the favored reaction mode for this specific catalyst type, is still underexplored and presents opportunities for addressing additional activation targets through XB-catalysis in the future.

Methods

General procedure for cycloaddition of aziridines with various dipolarophiles

Under an argon atmosphere, a dry 10 mL tube (screw cap with septum) was charged with **1a** (1.6 mg, 1.00 μmol, 1 mol% or 8.2 mg, 5.00 μmol, 5 mol% in case of alkenes as substrates) and aziridine **2** (0.100 mmol, 1.0 equiv.), evacuated three times, and backfilled with argon. Subsequently, DCM (1.0 mL) and the corresponding carbonyl **3** or alkyne **7** or alkene **10** (0.300 mmol, 3.0 equiv.) were added to the reaction mixture. The reaction was stirred until completion of the reaction (^{1}H-NMR analysis), nBu$_4$NBr (3.2 mg, 10.0 μmol, 10 mol%) was added, and the solvent was evaporated. The residue

was purified by column chromatography to give the desired N-heterocycles.

Computational details

All structures were preoptimized using a combination of XTB[71] and CREST[72,73] to evaluate the lowest energy conformers. The optimization and frequency analysis of these conformers were calculated using ORCA 6.0.1[74–78] with the ωB97X-D3BJ/def2-SVP[78–83] level of theory at room temperature (298 K). This combination was selected due to the complex binding nature of the σ-hole interactions, and its performance has been demonstrated with analogous systems.[84–87] The solvent effects, utilizing DCM as the solvent, were incorporated into the optimization through the implemented solvation model based on the density approach (SMD)[88] in ORCA 6.0.1 in its slightly modified version (SMD18)[89] with a corrected radius for iodine atoms. Single point energies were performed on the lowest energy small basis set calculations using ωb97X-D3BJ/def2-TZVP. Relative free energies (ΔG) were calculated as the energy difference between the complexes or the transition states (TS) and the sum of the energies of the reactants and the catalyst. Transition states were verified by the intrinsic reaction coordinate (IRC)[90] method as implemented in ORCA 6.0.1. The reaction energy diagram was initially created using EveRplot[91] and then modified with ChemDraw. The structures were visualized with CYLView[92] and the hydrogen atoms were omitted for clarity. The analysis of non-covalent interactions (NCI) was performed with NCIPlot[93–95] and visualized by VMD.[96] The coordinates of all calculated structures are given in the SI.

Conflicts of interest

There are no conflicts to declare.

Data availability

The data supporting this study, including detailed experimental procedures, spectroscopic data, and additional information, are available in the supplementary information (SI). Supplementary information: experimental procedures and the analytical data, including the corresponding NMR-spectra for unknown compounds and the Cartesian coordinates of the optimized structures from the DFT calculations. See DOI: **https://doi.org/10.1039/d5qo01119a**.

References

1 R. S. Spolar, J. H. Ha and M. T. Record, Hydrophobic effect in protein folding and other noncovalent processes involving proteins, *Proc. Natl. Acad. Sci. U. S. A.*, 1989, **86**, 8382–8385.
2 T. Young, R. Abel, B. Kim, B. J. Berne and R. A. Friesner, Motifs for molecular recognition exploiting hydrophobic enclosure in protein–ligand binding, *Proc. Natl. Acad. Sci. U. S. A.*, 2007, **104**, 808–813.
3 S. Jena, J. Dutta, K. D. Tulsiyan, A. K. Sahu, S. S. Choudhury and H. S. Biswal, Noncovalent interactions in proteins and nucleic acids: beyond hydrogen bonding and π-stacking, *Chem. Soc. Rev.*, 2022, **51**, 4261–4286.
4 V. A. Adhav and K. Saikrishnan, The Realm of Unconventional Noncovalent Interactions in Proteins: Their Significance in Structure and Function, *ACS Omega*, 2023, **8**, 22268–22284.
5 D. H. Williams, E. Stephens, D. P. O'Brien and M. Zhou, Understanding Noncovalent Interactions: Ligand Binding Energy and Catalytic Efficiency from Ligand-Induced Reductions in Motion within Receptors and Enzymes, *Angew. Chem., Int. Ed.*, 2004, **43**, 6596–6616.
6 H. He, W. Tan, J. Guo, M. Yi, A. N. Shy and B. Xu, Enzymatic Noncovalent Synthesis, *Chem. Rev.*, 2020, **120**, 9994–10078.
7 M. Raynal, P. Ballester, A. Vidal-Ferran and P. W. N. M. van Leeuwen, Supramolecular catalysis. Part 2: artificial enzyme mimics, *Chem. Soc. Rev.*, 2014, **43**, 1734–1787.
8 C. C. J. Loh, Exploiting non-covalent interactions in selective carbohydrate synthesis, *Nat. Rev. Chem.*, 2021, **5**, 792–815.
9 A. S. Mahadevi and G. N. Sastry, Cooperativity in Noncovalent Interactions, *Chem. Rev.*, 2016, **116**, 2775–2825.
10 A. J. Neel, M. J. Hilton, M. S. Sigman and F. D. Toste, Exploiting non-covalent π interactions for catalyst design, *Nature*, 2017, **543**, 637–646.
11 A. Haque, K. M. Alenezi, M. S. Khan, W.-Y. Wong and P. R. Raithby, Non-covalent interactions (NCIs) in π-conjugated functional materials: advances and perspectives, *Chem. Soc. Rev.*, 2023, **52**, 454–472.
12 J. Chen, Q. Peng, X. Peng, H. Zhang and H. Zeng, Probing and Manipulating Noncovalent Interactions in Functional Polymeric Systems, *Chem. Rev.*, 2022, **122**, 14594–14678.
13 L. Brunsveld, B. J. B. Folmer, E. W. Meijer and R. P. Sijbesma, Supramolecular Polymers, *Chem. Rev.*, 2001, **101**, 4071–4098.
14 G. R. Desiraju, Crystal Engineering: From Molecule to Crystal, *J. Am. Chem. Soc.*, 2013, **135**, 9952–9967.
15 M. Raynal, P. Ballester, A. Vidal-Ferran and P. W. N. M. van Leeuwen, Supramolecular catalysis. Part 1: non-covalent interactions as a tool for building and modifying homogeneous catalysts, *Chem. Soc. Rev.*, 2014, **43**, 1660–1733.
16 P. R. Schreiner, Metal-free organocatalysis through explicit hydrogen bonding interactions, *Chem. Soc. Rev.*, 2003, **32**, 289–296.
17 M. S. Taylor and E. N. Jacobsen, Asymmetric Catalysis by Chiral Hydrogen-Bond Donors, *Angew. Chem., Int. Ed.*, 2006, **45**, 1520–1543.
18 A. G. Doyle and E. N. Jacobsen, Small-Molecule H-Bond Donors in Asymmetric Catalysis, *Chem. Rev.*, 2007, **107**, 5713–5743.
19 X. Yu and W. Wang, Hydrogen-Bond-Mediated Asymmetric Catalysis, *Chem. – Asian J.*, 2008, **3**, 516–532.

20 M. Terada, Chiral Phosphoric Acids as Versatile Catalysts for Enantioselective Transformations, *Synthesis*, 2010, 1929–1982.
21 R. Maji, S. C. Mallojjala and S. E. Wheeler, Chiral phosphoric acid catalysis: from numbers to insights, *Chem. Soc. Rev.*, 2018, **47**, 1142–1158.
22 P. Metrangolo and G. Resnati, *Halogen bonding: fundamentals and applications*, Springer, 2008.
23 G. Cavallo, P. Metrangolo, R. Milani, T. Pilati, A. Priimagi, G. Resnati and G. Terraneo, The Halogen Bond, *Chem. Rev.*, 2016, **116**, 2478–2601.
24 L. Vogel, P. Wonner and S. M. Huber, Chalcogen Bonding: An Overview, *Angew. Chem., Int. Ed.*, 2019, **58**, 1880–1891.
25 D. Bulfield and S. M. Huber, Halogen Bonding in Organic Synthesis and Organocatalysis, *Chem. – Eur. J.*, 2016, **22**, 14434–14450.
26 R. L. Sutar and S. M. Huber, Catalysis of Organic Reactions through Halogen Bonding, *ACS Catal.*, 2019, **9**, 9622–9639.
27 J. Bamberger, F. Ostler and O. G. Mancheño, Frontiers in Halogen and Chalcogen-Bond Donor Organocatalysis, *ChemCatChem*, 2019, **11**, 5198–5211.
28 S. Huber, *Halogen Bonding in Solution*, John Wiley & Sons, 2020.
29 M. Breugst and J. J. Koenig, σ-Hole Interactions in Catalysis, *Eur. J. Org. Chem.*, 2020, 5473–5487.
30 G. Sekar, V. V. Nair and J. Zhu, Chalcogen bonding catalysis, *Chem. Soc. Rev.*, 2024, **53**, 586–605.
31 P. W. van Leeuwen and M. Raynal, *Supramolecular catalysis: new directions and developments*, John Wiley & Sons, 2021.
32 D. Jovanovic, M. Poliyodath Mohanan and S. M. Huber, Halogen, Chalcogen, Pnictogen, and Tetrel Bonding in Non-Covalent Organocatalysis: An Update, *Angew. Chem., Int. Ed.*, 2024, **63**, e202404823.
33 P. Metrangolo, F. Meyer, T. Pilati, G. Resnati and G. Terraneo, Halogen Bonding in Supramolecular Chemistry, *Angew. Chem., Int. Ed.*, 2008, **47**, 6114–6127.
34 L. C. Gilday, S. W. Robinson, T. A. Barendt, M. J. Langton, B. R. Mullaney and P. D. Beer, Halogen Bonding in Supramolecular Chemistry, *Chem. Rev.*, 2015, **115**, 7118–7195.
35 M. S. Taylor, Anion recognition based on halogen, chalcogen, pnictogen and tetrel bonding, *Coord. Chem. Rev.*, 2020, **413**, 213270.
36 R. Kampes, S. Zechel, M. D. Hager and U. S. Schubert, Halogen bonding in polymer science: towards new smart materials, *Chem. Sci.*, 2021, **12**, 9275–9286.
37 R. Wilcken, M. O. Zimmermann, A. Lange, A. C. Joerger and F. M. Boeckler, Principles and Applications of Halogen Bonding in Medicinal Chemistry and Chemical Biology, *J. Med. Chem.*, 2013, **56**, 1363–1388.
38 N. K. Shinada, A. G. de Brevern and P. Schmidtke, Halogens in Protein–Ligand Binding Mechanism: A Structural Perspective, *J. Med. Chem.*, 2019, **62**, 9341–9356.
39 S. H. Jungbauer, S. M. Walter, S. Schindler, L. Rout, F. Kniep and S. M. Huber, Activation of a carbonyl compound by halogen bonding, *Chem. Commun.*, 2014, **50**, 6281–6284.
40 J.-P. Gliese, S. H. Jungbauer and S. M. Huber, A halogen-bonding-catalyzed Michael addition reaction, *Chem. Commun.*, 2017, **53**, 12052–12055.
41 A. Dreger, P. Wonner, E. Engelage, S. M. Walter, R. Stoll and S. M. Huber, A halogen-bonding-catalysed Nazarov cyclisation reaction, *Chem. Commun.*, 2019, **55**, 8262–8265.
42 M. Damrath, A. Döring and B. J. Nachtsheim, Halogen bond-catalyzed Pictet–Spengler reaction, *Chem. Commun.*, 2025, **61**, 4828–4831.
43 M. V. Il'in, Y. V. Safinskaya, D. A. Polonnikov, A. S. Novikov and D. S. Bolotin, Chalcogen- and Halogen-Bond-Donating Cyanoborohydrides Provide Imine Hydrogenation, *J. Org. Chem.*, 2024, **89**, 2916–2925.
44 P. Wonner, A. Dreger, L. Vogel, E. Engelage and S. M. Huber, Chalcogen Bonding Catalysis of a Nitro-Michael Reaction, *Angew. Chem., Int. Ed.*, 2019, **58**, 16923–16927.
45 C. J. Vonnemann, E. Engelage, J. S. Ward, K. Rissanen, S. Keller and S. M. Huber, Ortho-Carborane-Derived Halogen Bonding Organocatalysts, *Angew. Chem., Int. Ed.*, 2025, e202424072, DOI: **10.1002/anie.202424072**.
46 F. Heinen, D. L. Reinhard, E. Engelage and S. M. Huber, A Bidentate Iodine(III)-Based Halogen-Bond Donor as a Powerful Organocatalyst, *Angew. Chem., Int. Ed.*, 2021, **60**, 5069–5073.
47 Z. Zhao, Y. Liu and Y. Wang, Weak Interaction Activates Esters: Reconciling Catalytic Activity and Turnover Contradiction by Tailored Chalcogen Bonding, *J. Am. Chem. Soc.*, 2024, **146**, 13296–13305.
48 X. Yuan and Y. Wang, A Selenide Catalyst for the Activation of Alkenes through Se···π Bonding, *Angew. Chem., Int. Ed.*, 2022, **61**, e202203671.
49 Y. Pang, Z. Zhao and Y. Wang, Activation of alkynes by chalcogen bonding: a Se···π interaction catalyzed intramolecular cyclization of 1,6-diynes, *Chem. Commun.*, 2023, **59**, 12278–12281.
50 H. Zhu, X. Yang, Y. Liu, H. Zhou and Y. Wang, Chalcogen Bonding Catalysis Enables Ring-Opening of Cyclopropene and Ring Expansion of Aryl Ketones, *Angew. Chem., Int. Ed.*, 2025, **64**, e202423746.
51 Z. Zhao and Y. Wang, Chalcogen Bonding Catalysis with Phosphonium Chalcogenide (PCH), *Acc. Chem. Res.*, 2023, **56**, 608–621.
52 A. L. Cardoso and T. M. V. D. Pinho e Melo, Aziridines in Formal [3 + 2] Cycloadditions: Synthesis of Five-Membered Heterocycles, *Eur. J. Org. Chem.*, 2012, 6479–6501.
53 X. E. Hu, Nucleophilic ring opening of aziridines, *Tetrahedron*, 2004, **60**, 2701–2743.
54 P. Lu, Recent developments in regioselective ring opening of aziridines, *Tetrahedron*, 2010, **66**, 2549–2560.
55 J.-J. Feng and J. Zhang, Synthesis of Unsaturated N-Heterocycles by Cycloadditions of Aziridines and Alkynes, *ACS Catal.*, 2016, **6**, 6651–6661.
56 H. Zhu, P.-P. Zhou and Y. Wang, Cooperative chalcogen bonding interactions in confined sites activate aziridines, *Nat. Commun.*, 2022, **13**, 3563.

57 F. Jiang, L.-Z. Zuo, H.-W. Zhao, S.-H. Xiang and B. Tan, Rational Design of an Organotellurium Chalcogen Bonding Catalyst for Azetidine Activation, *Angew. Chem., Int. Ed.*, 2025, e202511650.
58 A. Yoshimura and V. V. Zhdankin, Advances in Synthetic Applications of Hypervalent Iodine Compounds, *Chem. Rev.*, 2016, **116**, 3328–3435.
59 A. Yoshimura and V. V. Zhdankin, Recent Progress in Synthetic Applications of Hypervalent Iodine(III) Reagents, *Chem. Rev.*, 2024, **124**, 11108–11186.
60 F. V. Singh, S. E. Shetgaonkar, M. Krishnan and T. Wirth, Progress in organocatalysis with hypervalent iodine catalysts, *Chem. Soc. Rev.*, 2022, **51**, 8102–8139.
61 T. Wirth, *Hypervalent Iodine Chemistry*, Springer, 2016.
62 R. Robidas, D. L. Reinhard, C. Y. Legault and S. M. Huber, Iodine(III)-Based Halogen Bond Donors: Properties and Applications, *Chem. Rec.*, 2021, **21**, 1912–1927.
63 X. Peng, A. Rahim, W. Peng, F. Jiang, Z. Gu and S. Wen, Recent Progress in Cyclic Aryliodonium Chemistry: Syntheses and Applications, *Chem. Rev.*, 2023, **123**, 1364–1416.
64 D. Jovanovic and S. M. Huber, Cyclic Diaryliodonium Species as Synthetic Precursors and Halogen Bonding Organocatalysts, *Chem. Rev.*, 2023, **123**, 10527–10529.
65 A. Boelke, T. J. Kuczmera, L. D. Caspers, E. Lork and B. J. Nachtsheim, Iodolopyrazolium Salts: Synthesis, Derivatizations, and Applications, *Org. Lett.*, 2020, **22**, 7261–7266.
66 A. Boelke, T. J. Kuczmera, E. Lork and B. J. Nachtsheim, N-Heterocyclic Iod(az)olium Salts – Potent Halogen-Bond Donors in Organocatalysis, *Chem. – Eur. J.*, 2021, **27**, 13128–13134.
67 E. M. Galathri, T. J. Kuczmera, B. J. Nachtsheim and C. G. Kokotos, Organocatalytic Friedel–Crafts arylation of aldehydes with indoles utilizing N-heterocyclic iod(az)olium salts as halogen-bonding catalysts, *Green Chem.*, 2024, **26**, 825–831.
68 J. Su, Y. Liu, Y. Jing, Y. Liu and Z. Ke, Theoretical Quantification of the Lewis Acidity of N-Heterocyclic Iodonium Salts, *Asian J. Org. Chem.*, 2023, **12**, e202300210.
69 S. Teranishi, K. Maeda, T. Kurahashi and S. Matsubara, Diastereoselective Synthesis of 1,3-Oxazolidines via Cationic Iron Porphyrin-catalyzed Cycloaddition of Aziridines with Aldehydes, *Org. Lett.*, 2019, **21**, 2593–2596.
70 D. Crich and A. Banerjee, Chemistry of the Hexahydropyrrolo [2,3-b]indoles: Configuration, Conformation, Reactivity, and Applications in Synthesis, *Acc. Chem. Res.*, 2007, **40**, 151–161.
71 C. Bannwarth, E. Caldeweyher, S. Ehlert, A. Hansen, P. Pracht, J. Seibert, S. Spicher and S. Grimme, Extended tight-binding quantum chemistry methods, *Wiley Interdiscip. Rev.:Comput. Mol. Sci.*, 2021, **11**, e1493.
72 P. Pracht, F. Bohle and S. Grimme, Automated exploration of the low-energy chemical space with fast quantum chemical methods, *Phys. Chem. Chem. Phys.*, 2020, **22**, 7169–7192.
73 S. Grimme, Exploration of Chemical Compound, Conformer, and Reaction Space with Meta-Dynamics Simulations Based on Tight-Binding Quantum Chemical Calculations, *J. Chem. Theory Comput.*, 2019, **15**, 2847–2862.
74 F. Neese, The ORCA program system, *Wiley Interdiscip. Rev.: Comput. Mol. Sci.*, 2012, **2**, 73–78.
75 F. Neese, Software update: the ORCA program system, version 4.0, *Wiley Interdiscip. Rev.:Comput. Mol. Sci.*, 2018, **8**, e1327.
76 F. Neese, Software update: The ORCA program system—Version 5.0, *Wiley Interdiscip. Rev.:Comput. Mol. Sci.*, 2022, **12**, e1606.
77 F. Neese, F. Wennmohs, U. Becker and C. Riplinger, The ORCA quantum chemistry program package, *J. Chem. Phys.*, 2020, **152**, 224108.
78 A. Najibi and L. Goerigk, The Nonlocal Kernel in van der Waals Density Functionals as an Additive Correction: An Extensive Analysis with Special Emphasis on the B97M-V and ωB97M-V Approaches, *J. Chem. Theory Comput.*, 2018, **14**, 5725–5738.
79 J.-D. Chai and M. Head-Gordon, Long-range corrected hybrid density functionals with damped atom–atom dispersion corrections, *Phys. Chem. Chem. Phys.*, 2008, **10**, 6615–6620.
80 S. Grimme, J. Antony, S. Ehrlich and H. Krieg, A consistent and accurate ab initio parametrization of density functional dispersion correction (DFT-D) for the 94 elements H-Pu, *J. Chem. Phys.*, 2010, **132**, 154104.
81 S. Grimme, S. Ehrlich and L. Goerigk, Effect of the damping function in dispersion corrected density functional theory, *J. Comput. Chem.*, 2011, **32**, 1456–1465.
82 F. Weigend and R. Ahlrichs, Balanced basis sets of split valence, triple zeta valence and quadruple zeta valence quality for H to Rn: Design and assessment of accuracy, *Phys. Chem. Chem. Phys.*, 2005, **7**, 3297–3305.
83 F. Weigend, Accurate Coulomb-fitting basis sets for H to Rn, *Phys. Chem. Chem. Phys.*, 2006, **8**, 1057–1065.
84 N. Melnyk, M. R. Garcia and C. Trujillo, Halogen-Bond-Based Organocatalysis Unveiled: Computational Design and Mechanistic Insights, *ACS Catal.*, 2023, **13**, 15505–15515.
85 J. O'Brien, N. Melnyk, R. S. Lee, M. James and C. Trujillo, Computational Design of Bidentate Hypervalent Iodine Catalysts in Halogen Bond-Mediated Organocatalysis, *ChemPhysChem*, 2024, **25**, e202400515.
86 M. H. Kolář and P. Hobza, Computer Modeling of Halogen Bonds and Other σ-Hole Interactions, *Chem. Rev.*, 2016, **116**, 5155–5187.
87 S. Kozuch and J. M. L. Martin, Halogen Bonds: Benchmarks and Theoretical Analysis, *J. Chem. Theory Comput.*, 2013, **9**, 1918–1931.
88 A. V. Marenich, C. J. Cramer and D. G. Truhlar, Universal Solvation Model Based on Solute Electron Density and on a Continuum Model of the Solvent Defined by the Bulk Dielectric Constant and Atomic Surface Tensions, *J. Phys. Chem. B*, 2009, **113**, 6378–6396.
89 E. Engelage, N. Schulz, F. Heinen, S. M. Huber, D. G. Truhlar and C. J. Cramer, Refined SMD Parameters

for Bromine and Iodine Accurately Model Halogen-Bonding Interactions in Solution, *Chem. – Eur. J.*, 2018, **24**, 15983–15987.

90 K. Ishida, K. Morokuma and A. Komornicki, The intrinsic reaction coordinate. An ab initio calculation for HNC→HCN and H−+CH4→CH4+H−, *J. Chem. Phys.*, 1977, **66**, 2153–2156.

91 M. K. Bogdos and B. Morandi, EveRplot: A Web-Based Shiny Application for Creating Energy vs Reaction Coordinate Diagrams, *J. Chem. Educ.*, 2023, **100**, 3641–3644.

92 C. Y. Legault, 1.0b, Université de Sherbrooke, CYLview, 2009, **http://www.cylview.org**, (accessed 2025–08–04).

93 R. A. Boto, F. Peccati, R. Laplaza, C. Quan, A. Carbone, J.-P. Piquemal, Y. Maday and J. Contreras-García, NCIPLOT4: Fast, Robust, and Quantitative Analysis of Noncovalent Interactions, *J. Chem. Theory Comput.*, 2020, **16**, 4150–4158.

94 J. Contreras-García, E. R. Johnson, S. Keinan, R. Chaudret, J.-P. Piquemal, D. N. Beratan and W. Yang, NCIPLOT: A Program for Plotting Noncovalent Interaction Regions, *J. Chem. Theory Comput.*, 2011, **7**, 625–632.

95 E. R. Johnson, S. Keinan, P. Mori-Sánchez, J. Contreras-García, A. J. Cohen and W. Yang, Revealing Noncovalent Interactions, *J. Am. Chem. Soc.*, 2010, **132**, 6498–6506.

96 W. Humphrey, A. Dalke and K. Schulten, VMD - Visual Molecular Dynamics, *J. Mol. Graphics*, 1996, **14**, 33–38.